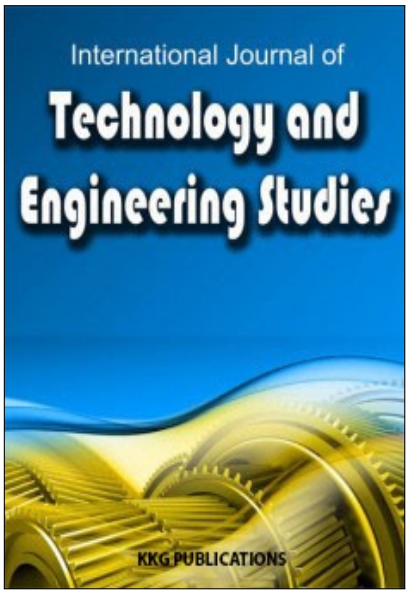

Key Knowledge Generation
Publication details, including instructions for author and subscription information:
http://kkgpublications.com/technology/

Free Bending Vibrations of Rotating Disks With A Concentric Hole

OLCAY OLDAC [1], MERTOL TUFEKCI [2], OMER EKIM GENEL [3], EKREM TUFEKCI [4]

[1, 2, 3, 4] Istanbul Technical University, Istanbul, Turkey

Published online: 28 December 2017

To cite this article: O. Oldac, M. Tufekci , O. E. Genel and E. Tufekci, "Free bending vibrations of rotating disks with a concentric hole," *International Journal of Technology and Engineering Studies,* vol. 3, no. 6, pp. 253-263, 2017.
DOI: https://dx.doi.org/10.20469/ijtes.3.40005-6

To link to this article: http://kkgpublications.com/wp-content/uploads/2017/3/IJTES-40005-6.pdf

PLEASE SCROLL DOWN FOR ARTICLE

KKG PUBLICATIONS

International Journal of Technology and Engineering Studies
vol. 3, no. 6, pp. 253-263, 2017

IJTES

FREE BENDING VIBRATIONS OF ROTATING DISKS WITH A CONCENTRIC HOLE

OLCAY OLDAC [1], MERTOL TUFEKCI [2*], OMER EKIM GENEL [3], EKREM TUFEKCI [4]

[1, 2, 3, 4] Istanbul Technical University, Istanbul, Turkey

Keywords:
Rotating Disk
Galerkin Method
Free Transverse Vibration
Campbell Diagrams

Received: 26 June 2017
Accepted: 13 September 2017
Published: 28 December 2017

Abstract. The main focus of this study is the dynamic behavior of rotating annular disks. The Galerkin method was used to determine the free vibration characteristics of rotating disks. In this method, the approximate function, that satisfies the boundary conditions for the solution, is selected and replaced by the differential equation of motion. Free vibrations of rotating disks, clamped at the inner circumference and free at the outer one, have been investigated. Also, Campbell diagrams are created to visualize system behavior. Solution of governing differential equations of the system is obtained by Galerkin method that includes proposing an approximate function for displacement that satisfies the boundary conditions. Two displacement functions are selected for the solution, and the boundary conditions are imposed to obtain the natural frequencies of the rotating disk. It is investigated how the dynamic behavior is affected by the disk's rotation speed in detail, and the results are visualized using Campbell diagrams drawn using dimensionless geometric parameters. Also, the solution method is validated using the results of the related studies in the literature.

INTRODUCTION

Due to having broad field of application in industry, rotating annular plates (disks) are one of the most common research topics in engineering. In the analysis of a disk brake squeal problem or cutting tool performance researches, understanding dynamical properties of a rotating disk plays a crucial role in engineering development process. Also, with the advancing technology, these disks are used in informatics sector to store data. One example of application areas is hard disks.

One of the first studies on rotating disks is given by Lamb and Southwell [1]. First nonlinear appoach is presented by Nowinski [2] using von Karman plate theory. Hamidzadeh [3] also worked on non-linear transverse free vibrations of rotating disks. Another notable work area about rotating disks is stability researches. Iwan and Moeller [4] and Yahnioglu and Akbarov [5] conducted researches about stability of rotating disks. They showed the unstable behavior of disk above the critical speeds in their work. Guven [6] represented a general solution of transverse vibrations of a rotating disk with equally distributed strength by using hypergeometric functions. Zhou et al. [7] applied Hamiltonian approach to investigate the natural vibrations of rotating disks. Also, Luo and Mote [8] investigated large amplitude vibrations of a storage device with a new approach.

In the literature, analytical studies about free vibrations of rotating disks are studied with Galerkin and Rayleigh-Ritz methods [9], [10], [11], [12]. Barasch and Chen [13] conducted a research with clamped and free boundary conditions in inner and outer edges, respectively. Their study is based on reduction of fourth order equation of motion to a system of differential equations. Bashmal et al. [14] investigated in-plane characteristics of non-rotating disks for various boundary conditions by using Rayleigh-Ritz method. Also, Tufekci et al. [15] conducted a research about transverse vibrational characteristics of a rotating disk under different boundary conditions by using Galerkin method. Maretic et al. [16] investigated vibrations and stability of rotating annular disks which are consisted of different materials under clamped and free boundary conditions at inner and outer edges, respectively. In order to obtain exact solution, they used Frobenius method. They also examined the effects of parameters such as angular velocity, Young modulus, and density on natural frequency. Renshaw [17] presented a method which is used to increase the natural frequencies of rotating disks via internal channels. He showed that thanks to well-designed channels, natural frequencies can be shifted 10%-100% above by comparing with uniform ones. Nejad et al. [18] obtained exact solution of rotating disk which is made of Functionally Graded Materials (FGM). They gave a closed form solution based on elasto-plastic analysis. They also studied on the behavior of the structure in plastic region at high speeds. Liu and Nayeb-Hashemi [19] presented a study about vibrational

*Corresponding author: Mertol Tufekci
†Email: tufekcime@itu.edu.tr

characteristics of a rotating disk which is made of FGM with circumferential crack. They investigated effects of crack parameters on critical speed. Kang [20] investigated axisymmetric oscillations of rotating annular disk with non-uniform thickness under tensile centrifugal body force with Ritz method. After performing classical plane elasticity approach and Ritz solution, obtained results are compared with other studies. In terms of experimental and numerical studies, papers by Bashmal et al. [21] and Tufekci et al. [22] can be given as examples. Bashmal et al. [21] conducted a research on annular disks which have different radius rates both numerically and experimentally. In their work, they emphasize that existence of non uniformities in boundary conditions has important role in the interaction between in-plane and transverse modes. Tufekci et al. [22] presented a study on vibrational characteristics of a hard disk both numerically and experimentally. Also, they validated their numerical results with analytical and experimental ones.

In this study, the Galerkin method was used to determine the free vibration characteristics of rotating disks. In this method, the approximate function, that satisfies the boundary conditions for the solution, is selected and replaced by the differential equation of motion. Free vibrations of rotating disks, clamped at the inner circumference and free at the outer one, have been investigated. Also, Campbell diagrams are created to visualize system behavior.

EQUATIONS

The differential equation of the vibration of the rotating disk in the coordinates connected to the disk is in the following form:

$$D\left(\frac{\partial^2}{\partial r^2}+\frac{1}{r}\frac{\partial}{\partial r}+\frac{1}{r^2}\frac{\partial^2}{\partial \varphi^2}\right)^2 w+\rho h\frac{\partial^2 w}{\partial t^2}- \frac{h}{r}\left[\frac{\partial}{\partial r}(\sigma_r r\frac{\partial w}{\partial r})+\frac{1}{r}\sigma_\varphi\frac{\partial^2 w}{\partial \varphi^2}\right]=0 \quad (1)$$

Here, w the transverse displacement function of the disk, D bending rigidity of the disk, E Young modulus, ν Poisson's ratio, σ_r and σ_φ are the radial and tangential stresses due to the rotation of the disk and change according to boundary conditions of the disk, (r, φ) the coordinates fixed to the disk. For the clamped and free boundary conditions at the inner and outer edges, respectively, the stresses are given as follows:

$$\sigma_r(r,\Omega)=\frac{(3+\nu)}{8}\rho\Omega^2(R_o^2-r^2)+ \frac{\rho\Omega^2R_i^2(1-\nu)\left[R_o^2(3+\nu)-R_i^2(1+\nu)\right]}{8\left[R_i^2(1-\nu)+R_o^2(1+\nu)\right]}\left(\frac{R_o^2}{r^2}+1\right) \quad (2)$$

$$\sigma_\varphi(r,\Omega)=\frac{\rho\Omega^2}{8}\left[(3+\nu)R_o^2-(1+3\nu)r^2\right]- \frac{\rho\Omega^2R_i^2(1-\nu)\left[R_o^2(3+\nu)-R_i^2(1+\nu)\right]}{8\left[R_i^2(1-\nu)+R_o^2(1+\nu)\right]}\left(\frac{R_o^2}{r^2}-1\right) \quad (3)$$

where Ω is the rotation speed of the disk, and R_2, R_o are the inner and outer radii of the disk, respectively.

The vertical displacement function of the disk according to the stationary coordinate system in the space is in the following form:

$$w(r,\psi,t)=\sum_{n=0}^{N}R_n(r)Sin(n\psi-\omega t) \quad (4)$$

where (r,ψ) are the fixed coordinates in space and n = 0,1,2,..., N.

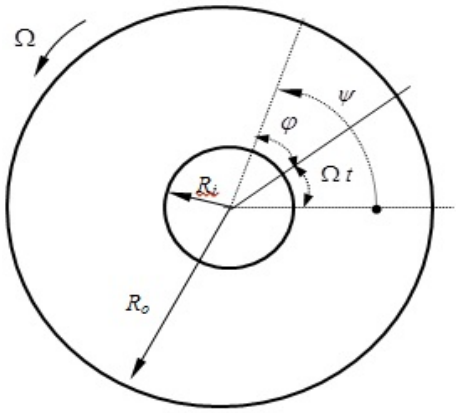

Fig. 1. Relationship between the coordinates fixed to disk and fixed in space

The modes expressed by this equation are called moving modes. ω shows the natural frequency of the disk, and n shows the number of circumferential waves. Substituting $\psi = \varphi + \Omega t$ into the equation, the coordinate system fixed in space can be switched to the system attached on to the disk:

$$w(r,\varphi,\Omega t,t) = \sum_{n=0}^{N} R_n(r) Sin(n\varphi + n\Omega t - \omega t) \tag{5}$$

$$w(r,\varphi,t) = \sum_{n=0}^{N} R_n(r) Sin\left[n\varphi + (n\Omega - \omega)t\right] \tag{6}$$

If (6) is substituted into (1), the following equation is obtained:

$$\sum_{n=0}^{n}\left\{D\left(\frac{d^2}{dr^2}+\frac{1}{r}\frac{d}{dr}-\frac{n^2}{r^2}\right)^2 R_n(r) - \rho h(n\Omega-\omega)^2 R_n r - \frac{h}{r}\left[\frac{d}{dr}\left(\sigma_r r\frac{dR_n(r)}{dr}\right)-\frac{n^2}{r}\sigma_\varphi R_n(r)\right]\right\}. \tag{7}$$
$$sin[n\varphi + (n\Omega-\omega)t] = 0$$

For each value of *n*, the term $sin[n\varphi + (n\Omega - \omega)t]$ may not be equal to zero. To satisfy this equality, the expression in parentheses must be zero.

$$D\left(\frac{d^2}{dr^2}+\frac{1}{r}\frac{d}{dr}-\frac{n^2}{r^2}\right)^2 R_n(r) - \rho h(n\Omega-\omega)^2 R_n r - \frac{h}{r}\left[\frac{d}{dr}\left(\sigma_r r\frac{dR_n(r)}{dr}\right)-\frac{n^2}{r}\sigma_\varphi R_n(r)\right] = 0 \tag{8}$$

Here, *n* = 0,1,2,..., *N*.

GALERKIN METHOD

The Galerkin method will be used for the solution. For this, an approximate function for the solution that satisfies the boundary conditions should be proposed. A function that provides boundary conditions can be selected as;

$$R_n(r) = \sum_{m=0}^{m} a_{mn} R_{mn}(r) \tag{9}$$

$$R_{mn}(r) = (r-R_i)^2[A_{mn}(r-R_i)^m + B_{mn}(r-R_i)^{m+1} + C_{mn}(r-R_i)^{m+2}] \tag{10}$$

where a_{mn} are unknown constants in the selected function for the solution A_{mn}, B_{mn} and C_{mn} are the coefficients that provide the boundary conditions. Also, the normalization condition is chosen as $R_{mn}(R_o) = 1$. Substituting the value of $R_n(r)$ in (10) into (8) will give the following equation;

$$\sum_{m=0}^{m}\left\{D\left(\frac{d^2}{dr^2}+\frac{1}{r}\frac{d}{dr}-\frac{n^2}{r^2}\right)^2 R_{nm}(r) - \rho h(n\Omega-\omega)^2 R_{nm}(r) - \frac{h}{r}\left[\frac{d}{dr}\left(\sigma_r r\frac{dR_{nm}(r)}{dr}\right)-\frac{n^2}{r}\sigma_\varphi R_{nm}(r)\right]\right\} = 0 \tag{11}$$

The weighted residual must be zero. So, the following equation can be obtained:

n = 0, 1, 2, 3, ..., N

$$\int_0^{2\pi}\int_{R_i}^{Ro}\left\{\sum_{m=0}^{m}\left[D\left(\frac{d^2}{dr^2}+\frac{1}{r}\frac{d}{dr}-\frac{n^2}{r^2}\right)^2 R_{nm}(r) - \rho h(n\Omega-\omega)^2 R_{nm}(r) - \frac{h}{r}\left[\frac{d}{dr}\left(\sigma_r r\frac{dR_{nm}(r)}{dr}\right)-\frac{n^2}{r}\sigma_\varphi R_{nm}(r)\right]\right]a_{mn}\right\}. \tag{12}$$
$$a_{sn}R_{sn}sin[n\varphi+(n\Omega-\omega)t]rdrd\varphi = 0$$

n = 0, 1, 2, ..., N *s = 0, 1, 2, ..., M*

In this equation, only the sine function is dependent on the angular coordinate φ. For this reason, the integral of this expression will be:

$$\int_0^{2\pi} sin\left[n\varphi + (n\Omega-\omega)t\right] d\varphi \tag{13}$$

Since this does not have to be necessarily equal to zero, (12) can be rewritten as follows;

$$\int_{R_i}^{Ro}\sum_{m=0}^{M}\left\{D\left(\frac{d^2}{dr^2}+\frac{1}{r}\frac{d}{dr}-\frac{n^2}{r^2}\right)^2 R_{mn}(r) - \rho h(n\Omega-\omega)^2 R_{mn}(r) - \frac{h}{r}\left[\frac{d}{dr}\left(\sigma_r r\frac{dR_{mn}(r)}{dr}\right)-\frac{n^2}{r}\sigma_\varphi R_{mn}(r)\right]\right\} a_{mn}a_{sn}R_{sn}rdr = 0 \tag{14}$$

n = 0, 1, 2, ..., N
s = 0, 1, 2, ..., M

Here, it is possible to change the order of summation and integral operations. By making this change, the following is obtained:

$$\sum_{m=0}^{M}\left[\frac{1}{\rho h}D\left[\int_{R_i}^{Ro}\left(\frac{d^2}{dr^2}+\frac{1}{r}\frac{d}{dr}-\frac{n^2}{r^2}\right)^2\right]R_{mn}\right]R_{sn}rdr$$
$$-h\int_{R_i}^{Ro}\left[\frac{d}{dr}\left(\sigma_r r\frac{dR_{mn}}{dr}\right)-\frac{n^2}{r}\sigma_\varphi R_{mn}\right]R_{sn}dr\Bigg\}\Bigg]A_{smn}=0$$
$$-(n\Omega-\omega)^2\int_{R_i}^{Ro}R_{mn}R_{sn}rdr\Bigg] \tag{15}$$

Where $A_{smn}=a_{mn}a_{sn}$.

The following abbreviations can be used to make this expression simpler:

$$\phi_{smn}=\frac{1}{\rho h}\Bigg\{D\int_{R_i}^{Ro}\left[\left(\frac{d^2}{dr^2}+\frac{1}{r}\frac{d}{dr}-\frac{n^2}{r^2}\right)^2R_{nm}\right]$$
$$R_{sn}dr-h\int_{R_i}^{Ro}\left[\frac{d}{dr}\left(\sigma_r r\frac{dR_{mn}}{dr}\right)-\frac{n^2}{r}\sigma_\varphi R_{mn}\right]R_{sn}dr\Bigg\} \tag{16}$$

$$\lambda_n=(n\Omega-\tau) \tag{17}$$

$$\Gamma_{smn}=\int_{R_i}^{Ro}R_{mn}R_{sn}rdr \tag{18}$$

For each value of *n*, the equation (13) gives a set of linear equations of dimension *(M + 1)* × *(M + 1)*. If the terms ϕ_{smn} and Γ_{smn} are used, equation becomes (17);

$$\sum_{m=0}^{M}\left[\phi_{smn}-\lambda^2\Gamma_{smn}\right]A_{smn}=0 \tag{19}$$

Removing the n index from the equation will make the equation simpler.

$$\sum_{m=0}^{M}\left[\phi_{smn}-\lambda^2\Gamma_{smn}\right]A_{smn}=0 \qquad s=0,1,2,.....M \tag{20}$$

n = 0, 1, 2,.....*N*

In order to find the solutions of each of system of linear equations obtained, the determinant of the coefficients matrix must be zero for every n. In other words, for each value of n, the natural frequencies are obtained by letting the determinant of 19 be zero:

$$det\left[\phi_{sm}-\lambda^2\Gamma_{sm}\right]=0 \qquad n=0,1,2,.....,N \tag{21}$$

$$\lambda=n\Omega-\omega \tag{22}$$

Equation (21) gives a polynom of λ^2 with the degree of *(M + 1)*. Roots are obtained as λ^2_{mn}. Natural frequencies of the rotating disk are obtained as follows:

$$\omega_{mn1,2}=n\Omega\mp\lambda_{mn} \tag{23}$$

As it can be seen from this equation, a non-rotating disk for each *(m, n)* value has only one frequency value. If the disk rotates, the frequency is divided into two different values in all other modes except *n* = 0 mode. These modes are called as travelling modes. As one of the waves travels in the direction of rotation, Forward Travelling Waves (FTW), the others travels in the opposite direction of rotation, Backward Travelling Waves (BTW). If the disk rotates, the natural frequencies of forward travelling waves increase and the natural frequencies of backward travelling waves decrease.

The results are given as dimensionless parameters. The dimensionless parameters are defined as:

$$\omega^*_{mn1,2}=\omega_{mn1,2}\left(\rho hR_o^6/D\right)^{1/2},$$
$$\Omega^*_{mn1,2}=\Omega_{mn1,2}\left(\rho hR_o^6/D\right)^{1/2} \tag{24}$$

Here, in order to obtain the frequency expression, the function $R_{mn}(r)$ must be determined. By using the boundary conditions, the constants A_{mn}, B_{mn}, and C_{mn} of the $R_{mn}(r)$ shape function will be easily determined.

The transverse displacement function of the disk given in (6) can be expressed as:

$$w=\sum_{n=0}^{N}\sum_{m=0}^{M}a_{mn}(r-R_i)^2[A_{mn}(r-R_i)^m+$$
$$B_{mn}(r-R_i)^{m+1}+C_{mn}(r-R_i)^{m+2}].sin[n\phi(n\Omega-\omega t)] \tag{25}$$

This function must satisfy the boundary conditions of disk.

It is also possible to select another $R_{mn(r)}$ function which satisfies the boundary conditions of the disk as follows:

$$R_{mn}(r)=X^1_{mn}r_o^m+X^2_{mn}r_o^{m+1}+X^3_{mn}r_o^{m+2}+$$
$$X^4_{mn}r_o^{m+3}+X^5_{mn}r_o^{m+4} \tag{26}$$

$X^1_{mn}, X^2_{mn}, X^3_{mn}, X^4_{mn}$ are unknown constants and will be calculated using the boundary conditions of the disk and the normalization condition.

When the function of $R_{mn}(r)$ is substituted into the transverse displacement function of the disk *w*, the following is obtained:

$$w = \sum_{n=0}^{N}\sum_{m=0}^{M} r_{mn}(r) = (X_{mn}^{1}r^{m} + X_{mn}^{2}r^{m+1} + X_{mn}^{3}r^{m+2} + X_{mn}^{4}r^{m+3} + X_{mn}^{5}r^{m+4})sin\left[(n\psi - \omega t)\right] \quad (27)$$

The disk is clamped at the inner circumference, free at the outer circumference. The boundary condition at the inner circumference; - There will be no displacement:

$$w\big|_{r=R_i} = 0 \quad (28)$$

- There will be no angle of rotation:

$$\left.\frac{\partial w}{\partial r}\right|_{r=R_o} = 0 \quad (29)$$

Boundary conditions in the outer circumference;
- The moment value at the free edge will be zero:

$$m_r(R_o) = 0 = -D\left(\frac{\partial^2 w}{\partial r^2} + \frac{\nu}{r}\frac{\partial w}{\partial r} + \frac{\nu}{r^2}\frac{\partial^2 w}{\partial \varphi^2}\right)\Big|_{r=R_o} = 0 \quad (30)$$

- The equivalent shear force value at the free edge will be zero:

$$V_r(R_0) = 0 - D\left(\frac{\partial^3 w}{\partial r^3} - \frac{3-\nu}{r^3}\frac{\partial^2 w}{\partial \varphi^2} + \frac{2-\nu}{r^2}\frac{\partial^3 w}{\partial r \partial \varphi^2} - \frac{1}{r^2}\frac{\partial w}{\partial r} + \frac{1}{r}\frac{\partial^2 w}{\partial r^2}\right)\Big|_{r=R_o} = 0 \quad (31)$$

Normalization condition is given by the equation below;

$$R_{mn}(R_o) = 1 \quad (32)$$

$$X_{mn}^{1}R_o^{m} + X_{mn}^{2}R_o^{m+1} + X_{mn}^{3}R_o^{m+2} + X_{mn}^{4}R_o^{m+3} + X_{mn}^{5}R_o^{m+4} \quad (33)$$

Therefore, the normalization condition will be used with the free edge boundary conditions at the outer circle to determine the indefinite constants A_{mn}, B_{mn}, and C_{mn}. If these equations are written in matrix form, it will take the following form:

$$\begin{bmatrix} A_{00}^{11} & A_{00}^{12} & A_{00}^{13} & A_{00}^{14} & A_{00}^{15} & & & & & & & & & & \\ A_{00}^{21} & A_{00}^{22} & \cdots & \cdots & A_{00}^{25} & & & & & & & & & & \\ A_{00}^{31} & \cdots & \cdots & \cdots & \cdots & & & & & & & & & & \\ A_{00}^{41} & \cdots & \cdots & \cdots & \cdots & & & & & & & & & & \\ A_{00}^{51} & \cdots & \cdots & \cdots & A_{00}^{55} & & & & & & & & & & \\ & & & & & A_{01}^{11} & A_{01}^{12} & A_{01}^{13} & A_{01}^{14} & A_{01}^{15} & & & & & \\ & & & & & A_{01}^{21} & \cdots & \cdots & \cdots & \cdots & & & & & \\ & & & & & A_{01}^{31} & \cdots & \cdots & \cdots & \cdots & & & & & \\ & & & & & A_{01}^{41} & \cdots & \cdots & \cdots & \cdots & & & & & \\ & & & & & A_{01}^{51} & \cdots & \cdots & \cdots & A_{01}^{55} & & & & & \\ & & & & & & & & & & A_{02}^{11} & \cdots & A_{02}^{15} & & \\ & & & & & & & & & & A_{02}^{51} & \cdots & A_{02}^{55} & & \\ & & & & & & & & & & & \ddots & & & \\ & & & & & & & & & & & & A_{0M}^{11} & \cdots & A_{0M}^{15} \\ & & & & & & & & & & & & A_{0M}^{51} & \cdots & A_{0M}^{55} \\ & & & & & & & & & & & & & A_{10}^{11} & \cdots & A_{10}^{15} \\ & & & & & & & & & & & & & A_{10}^{51} & \cdots & A_{10}^{55} \\ & & & & & & & & & & & & & & & \ddots \end{bmatrix} \begin{bmatrix} X_{00}^{1} \\ X_{00}^{2} \\ X_{00}^{3} \\ X_{00}^{4} \\ X_{00}^{5} \\ X_{01}^{1} \\ X_{01}^{2} \\ \vdots \\ X_{01}^{5} \\ \vdots \\ X_{0M}^{5} \\ X_{10}^{1} \\ \vdots \\ X_{10}^{5} \\ \vdots \\ X_{NM}^{1} \\ X_{NM}^{2} \\ \vdots \\ X_{NM}^{5} \end{bmatrix} = \begin{bmatrix} 0 \\ 0 \\ 0 \\ 0 \\ 1 \\ 0 \\ 0 \\ 0 \\ 0 \\ 1 \\ 0 \\ 0 \\ 0 \\ 0 \\ \vdots \\ \vdots \\ \vdots \\ 0 \\ 1 \\ 0 \\ 0 \\ 0 \\ 0 \\ 0 \\ 1 \end{bmatrix} \quad (34)$$

RESULTS

Natural Frequencies, Mode Shapes and Campbell Diagrams

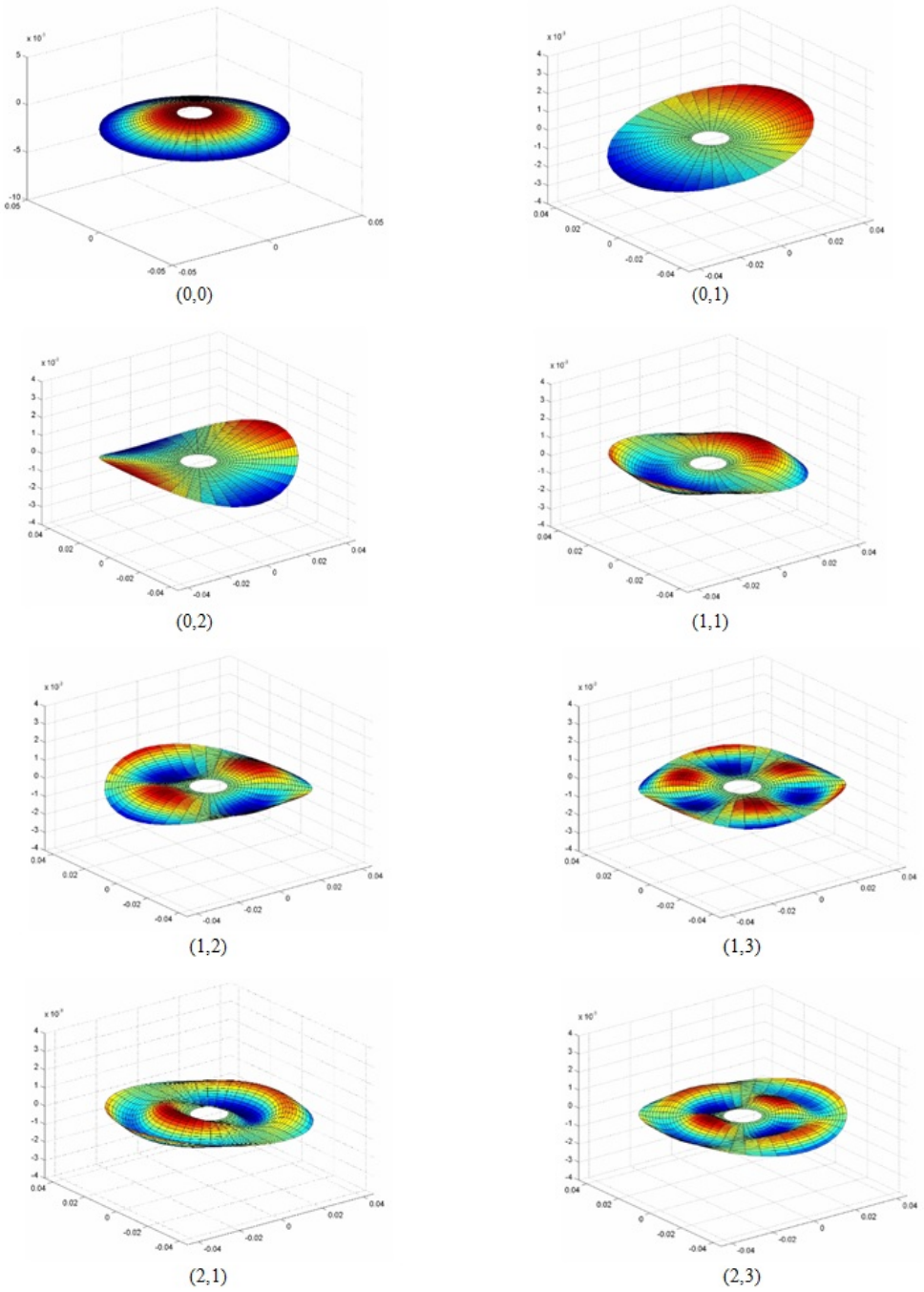

Fig. 2. Some mode shapes of rotating disk

After all, the calculations are performed using the above-mentioned solution methods. The calculations yield the natural frequencies and mode shapes of the disk rotating at various angular velocities. Outputs of the calculations are visualized for better understanding. For visualization, Campbell diagrams are plotted by a program written in MATLAB and also mode shapes are drawn using the 3D plotting tools of the same software.

Some mode shapes are given in Figure 2. In this Figure,

mode (0, 0) is called "umbrella mode" due to not having any nodal diameter ($n = 0$). Also, it can be observed that, at specific radii, transverse displacements of points are zero for non-zero values of nodal circle ($m \neq 0$).

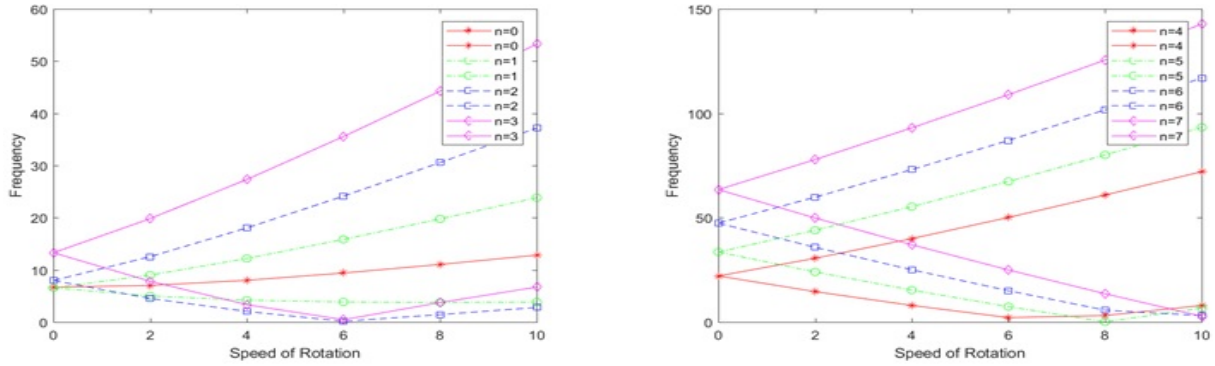

Fig. 3. Campbell diagrams for $m = 0$

In order to express structural behavior more clearly, Campbell diagrams are plotted at different speed for various nodal circle (m) and nodal diameter (n) values. These diagrams are shown in Figures 3-6.

The changes of the dimensionless natural frequencies with varying dimensionless rotation speed are given in Figure 3 for $m = 0$, Figure 4 for $m = 1$, Figure 5 for $m = 2$ and Figure 6 for $m = 3$. As shown in all Figures, except for $n = 0$ mode, the dimensionless frequencies are divided into two different values for increasing dimensionless speed of rotation in all other mode shapes. These frequencies are related to the so called traveling modes as mentioned before. Natural frequencies of the backward traveling modes for $n \neq 0$ decrease until zero with the decreasing rotation speed. This rotation speed is called a ritical speed. Any outer disturbance can easily initiate the resonance phenomena in the disk and lead the structure to instant or progressive fatigue failure. In Figure 3, it is to be noticed that there are critical speeds detected in backward traveling modes of n = 2-4 around the rotation speed of 6-7 while the critical speed of mode 5 is around the rotation speed of 8. For higher modes of n, the critical speeds are to be seen in much higher rotation speeds. It is also interesting to note that the critical speed is not observed for the mode of $n = 1$.

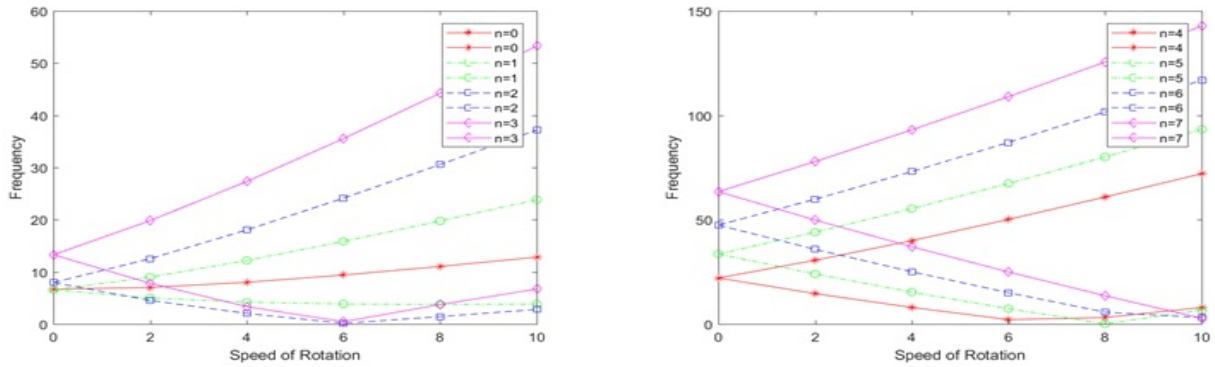

Fig. 4. Campbell diagrams for $m = 1$

In order to express structural behavior more clearly, Campbell diagrams are plotted at different speed for various nodal circle (m) and nodal diameter (n) values. These diagrams are shown in Figures 3-6.

The changes of the dimensionless natural frequencies with varying dimensionless rotation speed are given in Figure 3 for $m = 0$, Figure 4 for $n = 1$, Figure 5 for $m = 2$ and Figure 6 for $m = 3$. As shown in all figures, except for $n = 0$ mode, the

dimensionless frequencies are divided into two different values for increasing dimensionless speed of rotation in all other mode shapes. These frequencies are related to the modes so called travelling modes as mentioned before. Natural frequencies of the backward travelling modes for $n \neq 0$ decrease until zero with the decreasing rotation speed. This rotation speed is called a "critical speed". Any outer disturbance can easily initiate the resonance phenomena in the disk and lead the structure to instant or progressive fatigue failure. In Figure 3, it is to be noticed that there are critical speeds detected in backward travelling modes of n = 2-4 around the rotation speed of 6-7 while the critical speed of mode 5 is around the rotation speed of 8. For higher modes of n, the critical speeds are to be seen in much higher rotation speeds. It is also interesting to note that the critical speed is not observed for the mode of n = 1.

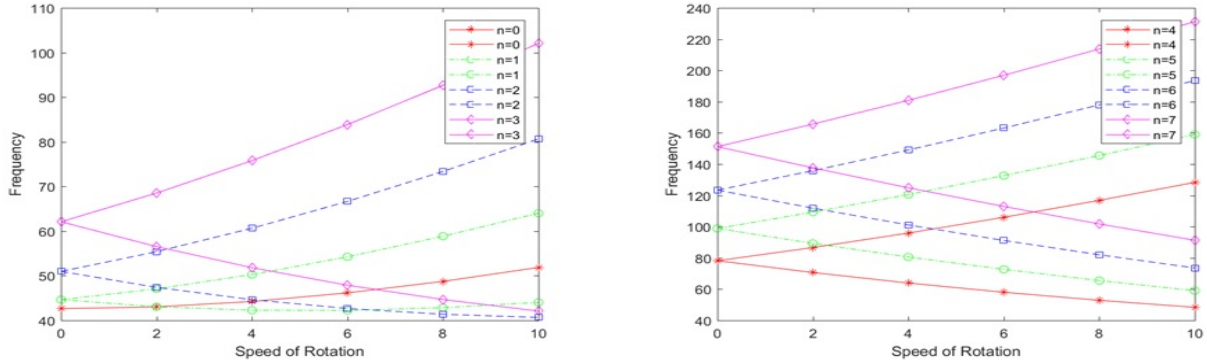

Fig. 5. Campbell diagrams for m = 1

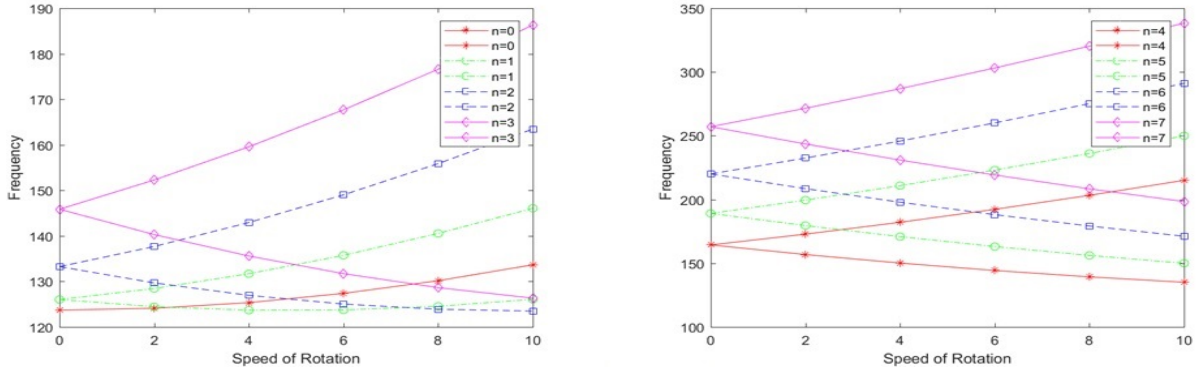

Fig. 6. Campbell diagrams for m = 2

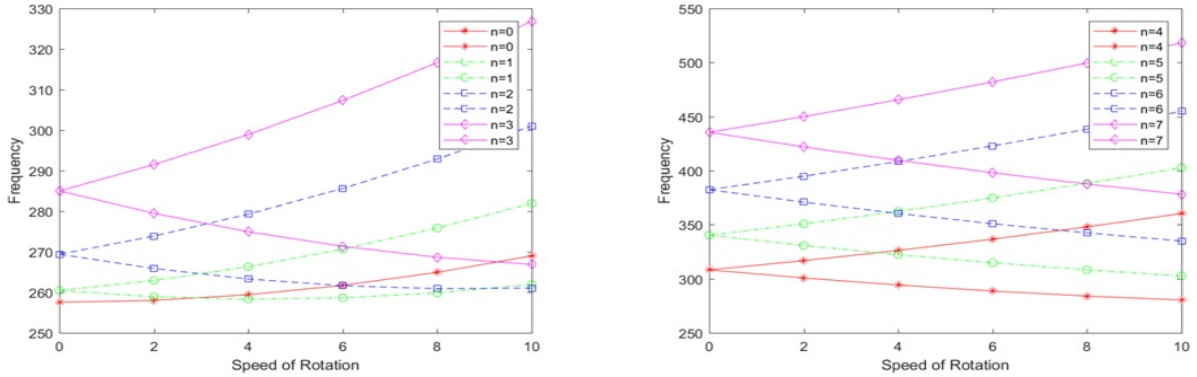

Fig. 7. Campbell diagrams for m = 3

For non-zero values of nodal circle ($m \neq 0$) in Figures 4-6, the critical speeds are not observed even for higher modes of n.

It can also be easily seen from Figures 3-6, the values of natural frequencies increase for each value of n with increasing values of m and also a rise is to be observed in natural frequencies for each m value increasing values of n.

The difference between forward and backward travelling waves for each mode can be seen more distinctly with the increasing rotation speed. This difference becomes more significant for higher nodal diameter, n values. At certain rotational speed values, they are intersected. Since there is no nodal diameter in $n = 0$ mode, there will be no forward or backward travelling wave. Therefore, two frequency values, except for this mode, for each mode are obtained at each rotation speed value. Depending on the rotation speed, the natural frequencies are obtained and the Campbell diagrams are plotted. Campbell diagrams have been compared with and matched the results given in the literature [8], [10], [12], [14]. Campbell diagrams are available in the literature for the values 0 and 1 of the number of nodal circles (m).

In this study, the diagrams are also drawn for $m = 2$ and 3. Campbell diagrams are presented in Figures 5 and 6 for various nodal circles and nodal diameters.

The order of the modes of stationary disk changes when the rotation speed increases. For example, in Figure 3, the frequency of the backward traveling wave of the mode $n = 3$ are smaller than those of $n = 0$ and 1 for the case when the dimensionless rotation speed is given as 5.

DISCUSSION

For a stationary disk, there is only one natural frequency for each mode. But when rotation speed increases, the natural frequency is separated into two parts; one for the backward travelling wave, one for the forward traveling wave. This separation phenomenon is a crucial part of dynamic behavior of rotating systems and has to be predicted precisely in order to prevent unexpected vibrations with significant effects on the system or even failure.

The measured results in[20] are used in order to validate presented analytical approach. In [20], the natural frequencies of DISK III made of aluminum are measured. The inner and outer radii of the disk are 0.02 m and 0.15 m, respectively. The density of the aluminum is 2680 kg/m^3 and the Young's modulus is 15 Gpa. Also the rotation speed of the disk is 1920 rpm. The measured frequencies for the first two modes of the rotating disk are given as 7.68 kHz and 7.73 kHz. Using these geometric and material properties, analytical results are calculated as 8290.9 Hz and 8354.9 Hz. Absolute percentage errors between experimental and analytical natural frequencies are 7.95% and 8.08%, respectively. Both frequencies calculated in this study are larger than the experimental ones. These differences between the results are caused by idealized conditions in the analytical study. In the experiments, there are almost several uncertinites in boundary conditions, material, and geometric properties to some extent. These will cause such a difference. The comparison shows that analytical results are in good agreement with experimental results given in [20].

Another validation is done by [21] in which the natural frequencies of transverse vibrations of the hard disk are measured and simulated using Finite Element Method (FEM). These results are compared with analytical values, which were calculated using presented method in this paper, to investigate the validity of the approach. Compared results which include stationary, rotating including FTW and BTW travelling modes for (0, 2) and (0, 3) are presented in Table 1. It can be seen from Table 1 that analytical natural frequencies are compatible with experimental and numerical results for stationary case, FTW and BTW. For mode 3 and mode 4, maximum absolute percentage errors between analytical and experimental results are 1.77% and 4.03%, respectively. Both of these errors exist in backward traveling waves at 2000 rpm. Also, maximum absolute percentage errors between analytical and numerical results are 0.74% and 0.81%, respectively. These errors occur in backward traveling waves in 8000 rpm. Therefore, it can be said that the analytical results are in good agreement with experimental and numerical ones.

The agreement of analytical results is stronger with numerical results than the experimental results. The reason for it can be stated as the similar idealization of boundary conditions used in both numerical and analytical calculations. In the experimental study, there are other parameters that affect the natural frequencies, such as uncertainties in boundary conditions, material and geometrical properties, etc. But, these uncertainties cannot be taken into account in analytical and numerical studies. Instead of including those uncertainties that affect significantly the experimental results, idealization assumptions are made in boundary condition, material properties etc.

TABLE 1
COMPARISON OF ANALYTICAL RESULTS WITH EXPERIMENTAL AND NUMERICAL RESULTS [21]

		MODE 3 (0,2) (Hz)			MODE 4 (0,3) (Hz)		
Rotation Speed (rpm)	Wave Type	Experimental [21]	Numerical [21]	Analytical This Study	Experimental [21]	Numerical [21]	Analytical This Study
0	-	1232	1211.47	1218.80	1830	1878.12	1890,44
2000	FTW	1301	1279.22	1286.54	1921	1979.18	1991.49
	BTW	1174	1145.88	1153.21	1722	1779.18	1791.49
4000	FTW	1350	1349.14	1356.44	2032	2082.33	2094.63
	BTW	1101	1082.48	1089.78	1641	1682.33	1694.63
6000	FTW	1424	1421.21	1428.49	2137	2187.59	2199.85
	BTW	1044	1021.21	1028.49	1544	1587.59	1599.85
8000	FTW	1484	1495.40	1502.64	2245	2294.92	2307.14
	BTW	971	962.06	969.31	1454	1494.92	1507.14

CONCLUSION AND RECOMMENDATIONS

In this paper, transverse free vibrations of rotating annular disks are investigated with analytical approach. In order to obtain the natural frequencies, the equation of motion is formulated. Boundary conditions are taken as clamped and free in inner and outer circumferences, respectively, which is similar to the fixtures of hard disks. Then, solution of equation of motion is done with Galerkin method, one of the most well-known solution techniques. Two different polynomial functions, which satisfy the boundary conditions, are chosen as the approximate solution of equation of motion. The unknown coefficients are obtained from the boundary and normalization conditions. Then the natural frequencies are calculated. The same results are obtained by using these two approximate functions. For presenting structural behavior clearly, obtained results are plotted in Campbell diagrams, which represent the frequency versus the rotation speed of the disk for different nodal diameter and nodal circle values. As it is well-known, it can be seen from the diagrams for a stationary disk that each mode has only one natural frequency. Also, for a rotating disk, each mode without nodal diameter has only one natural frequency for each rotation speed. However, in all modes of a rotating disk with nodal diameters, two distinct natural frequency values are observed. The diagrams are in good agreement with those given in the literature. Critical speed is the rotation speed in which the frequency of the BTW becomes zero. In this rotation speed, the resonance can be initiated by any disturbance and the undesirable behavior or even failure may occur.

In cases where $m = 0$ and $n = 2, 3, 4$, critical speeds can easily be observed. However, for modes where $m = 0$ and $n = 0, 1$, there will be no critical speed to be observed. For higher values of m, the critical speeds are not to be practically observed. The natural frequencies and critical speeds are far beyond the practical limits. Therefore, the modes of higher values of m are not significant for practical applications.

Also, for validation purposes, the results of analytical approach are compared with the experimental and numerical results of two different studies and comparison is given in a table. It is shown that the results of this study are in good agreement with those in the literature.

The results of this study are in excellent agreement with numerical results. The differences between the results of this study and the experimental study given in the literature are a bit higher than those of this study and the numerical ones in the literature. Since the analytical and numerical calculations use some idealizations for the boundary conditions, material and geometric parameters, etc. In the experimental study, there are some uncertainties in these parameters which affect the measured results.

Declaration of Conflicting Interests

There are no conflicts of interest in this work.

REFERENCES

[1] H. Lamb and R. V. Southwell, "The vibrations of a spinning disk," *Royal Society of Publishing* vol. 99, no. 669, pp. 272-280, 1921.

[2] J. L. Nowinski, "Nonlinear transverse vibrations of a spinning disk," *Journal of Applied Mechanics,* vol. 31, no. 1, pp. 72-78, 1964.

[3] H. R. Hamidzadeh, "Non-linear free transverse vibration of thin rotating discs," *Journal of Multi-body Dynamics, Part K: Journal of Multi-body Dynamics,* vol. 221, no. 3, pp. 467-473, 2007

[4] W. D. Iwan and T. L. Moeller, "The stability of a spinning elastic disk with a transverse load system," *Journal of Applied Mechanics,* vol. 43, no. 3, pp. 485-490, 1976.

[5] Z. Kutug, . Yahnioglu and S. D. Akbarov, "The loss of stability analyses of an elastic and viscoelastic composite circular plate in the framework of three-dimensional linearized theory of stability," *International Journal of Mechanical Sciences,* vol. 22, no. 3, pp. 475-488, 2002.

[6] U. Guven, "On transverse vibrations of a rotating disk uniform strength," *Journal of Applied Mechanics,* vol. 59, no. 1, pp. 234-235, 1992.

[7] Z. H. Zhou, K. W. Wong, X. S. Xu and A. Y. T. Leung, "Natural vibration of circular and annular thin plates by Hamiltonian approach," *Journal of Sound and Vibration,* vol. 330, no. 5, pp. 1005-1017, 2011.

[8] A. C. J. Luo and C. D. Mote, "Nonlinear vibration of rotating thin disks," *ASME Journal of Vibration and Acoustics,* vol. 122, no. 4, pp. 376-383, 2000.

[9] G. K. Ramaiah, "Natural frequencies of spinning annular plates," *Journal of Sound and Vibration,* vol. 74, no. 2, Pp. 303-310, 1981.

[10] K. N. Koo, "Vibration analysis and critical speeds of polar orthotropic annular disks in rotation," *Composite Structures,* vol. 76, no. 1, pp. 67-72, 2006.

[11] H. L. Pei, Y. C. Tan and S. Jiang, "Modal interactions of rotating flexible disc," *Journal of Mechanical Engineering Science,* vol. 225, no. 12, pp. 2819-2830, 2011.

[12] S. Barasch and Y. Chen, "On the vibration of a rotating disk," *Journal of Applied Mechanics,* vol. 39, no. 4, pp. 1143-1144, 1972.

[13] S. Bashmal, R. Bhat and S. Rakheja, "In-plane free vibration of circular annular disks," *Journal of Sound and Vibration,* vol. 322, no. 1, pp. 216226, 2009.

[14] M. Tufekci, H. Ko, O. E. Genel, O. Oldac and E. Tufekci "Free vibrations of rotating discs," in *20th National Mechanical Congress,* Uludag University, Bursa, Turkey, September 05-09 2017.

[15] R. Maretic, V. Glavardanov and V. Milosevic-Mitic, "Vibration and stability of rotating annular disks composed of different materials," *Archive of Applied Mechanics,* vol. 85, no. 1, pp. 117-131, 2014.

[16] A. A. Renshaw, "Increasing the natural frequencies of circular disks using internal channels," *Journal of Sound and Vibration,* vol. 229, no. 2, pp. 355-375, 2000.

[17] M. Z. Nejad, A. Rastgoo and A. Hadi, "Exact elasto-plastic analysis of rotating disks made of functionally graded materials," *International Journal of Engineering Science,* vol. 85, pp. 47-57, 2014

[18] R. Liu and H. Nayeb-Hashemi, "Vibration response of functionally graded rotating disk with a circumferential crack," in *ASME Conference of International Mechanical Engineering Congress and Exposition,* British Columbia, Canada, pp. 35-40, 2010.

[19] J. H. Kang, "Axisymmetric vibration of rotating annular plate with variable thickness subjected to tensile centrifugal body force," *International Journal of Structural Stability and Dynamics,* vol. 17, no. 09, pp. 175-192, 2017

[20] S. Bashmal, R. Bhat and S. Rakheja, "Experimental and numerical study of the vibration of stationary and rotating annular disks," *Journal of Vibration and Acoustics,* vol. 138, no. 5, pp. 1-11, 2016.

[21] M. Tufekci, O. E. Genel and O. Oldac, "Finite element and experimental analysis of vibrations of a rotating disc", in *Tokyo 18th International Conference on Engineering & Technology, Computer, Basic & Applied Sciences,* Tokyo, Japan, 2017.

— This article does not have any appendix. —